

Nanostructured Polymers Enable Stable and Efficient Low-Power Photon Upconversion

Felipe Saenz, Alessandra Ronchi, Michele Mauri, Roberto Vadrucci, Francesco Meinardi, Angelo Monguzzi, and Christoph Weder*

Photon upconversion based on sensitized triplet–triplet annihilation (sTTA-UC) is a wavelength-shifting technique with potential use in actuators, sensing, and solar technologies. In sTTA-UC, the upconverted photons are the result of radiative recombination of high-energy singlets, which are created through the fusion of metastable triplets of two annihilator/emitter molecules. The emitter triplets are populated via energy transfer (ET) from a low-energy absorbing light-harvester/sensitizer. The process is highly efficient at low powers in solution but becomes relatively ineffective in solid matrices since the limited molecular mobility precludes bimolecular interactions. The realization of efficient solid-state upconverters that exhibit long-term stability and are compatible with industrial fabrication processes is an open challenge. Here, nanophase-separated polymer systems synthesized under ambient conditions that contain the upconverting dyes in liquid nanodomains is reported. The nanostructured polymers show an excellent optical quality, an outstanding upconversion efficiency of up to $\approx 23\%$, and excellent stability in air, with only negligible performance losses over a period of three months. Moreover, the dyes' confinement in nanosized domains < 50 nm results in an increased effective local density of chromophores that enables hopping-assisted ET and TTA and confers to the upconversion process peculiar kinetics that enhances the material performance at low powers.

upconverted fluorescence in sTTA-UC is the result of the fusion of the metastable triplets of two annihilator/emitter molecules upon collision, which results in the formation of a high-energy singlet excited state that decays radiatively. The emitter triplets are populated via Dexter energy transfer (ET) from the triplets of a low-energy absorbing moiety, that is, a light-harvester/sensitizer (Figure S1, Supporting Information).^[2] The realization of solid-state upconverting materials that display high efficiency, low power threshold, and good long-term stability, and which can be manufactured in a technologically exploitable manner, is one of the open challenges in the field. Many dye pairs exhibit a high upconversion yield in solution, where large molecular diffusivities render ET and TTA highly effective, but they are relatively inefficient when incorporated in solid matrices where molecular mobility is typically low.^[3] Nevertheless, solid materials are better suited for integration into technologically useful devices, which motivates the development of methods to circumvent the constraints associated with sTTA-UC in a rigid medium.

1. Introduction

Photon upconversion based on sensitized triplet–triplet annihilation (sTTA-UC) is a promising wavelength-shifting strategy that is potentially useful for applications such as actuators, sensors, or to enhance the light harvesting ability of photovoltaic devices by recovering sub-bandgap solar photons.^[1] The


constraints associated with sTTA-UC in a rigid medium. In recent years, different approaches have been explored to develop solid upconverting materials, including upconverting nanoparticles, macromolecular self-assemblies, dye doped polymers, organic glasses, gels, and others.^[4] Each of these approaches has advantages and drawbacks, and it is still challenging to combine all of the characteristics required for a material to be technologically useful, that is, high chromophore density, protection from oxygen, high efficiency, high stability, tunable mechanical properties, ease of fabrication, and economical starting materials.

Recently, some of us have introduced nanophase-separated polymers that contain a glassy matrix and a liquid upconverting phase as an attractive platform to create sTTA-UC materials.^[5] The materials were accessed by the in-situ formation of a phase-separated architecture featuring a liquid upconverting phase within a solid, cross-linked polymeric matrix. The liquid phase, stabilized by a surfactant, was based on a non-polar solvent in which the upconverting dyes are dissolved, whereas the polymer matrix was formed by polar monomers and optionally a cross-linker. Upconverters made by this approach exhibited intriguing properties; the liquid nature of the upconverting phase led to a high upconversion yield, while the polymer matrix provided rather effective

F. Saenz, Prof. C. Weder
Adolphe Merkle Institute
University of Fribourg
Fribourg CH-1700, Switzerland
E-mail: christoph.weder@unifr.ch

A. Ronchi, Dr. M. Mauri, Prof. F. Meinardi, Prof. A. Monguzzi
Dipartimento di Scienza dei Materiali
Università degli Studi Milano-Bicocca
Via Roberto Cozzi 55, Milano 20125, Italy

Dr. R. Vadrucci
BASF
Carl-Bosch-Strasse 38, Ludwigshafen am Rhein 67056, Germany

 The ORCID identification number(s) for the author(s) of this article can be found under <https://doi.org/10.1002/adfm.202004495>.

DOI: 10.1002/adfm.202004495

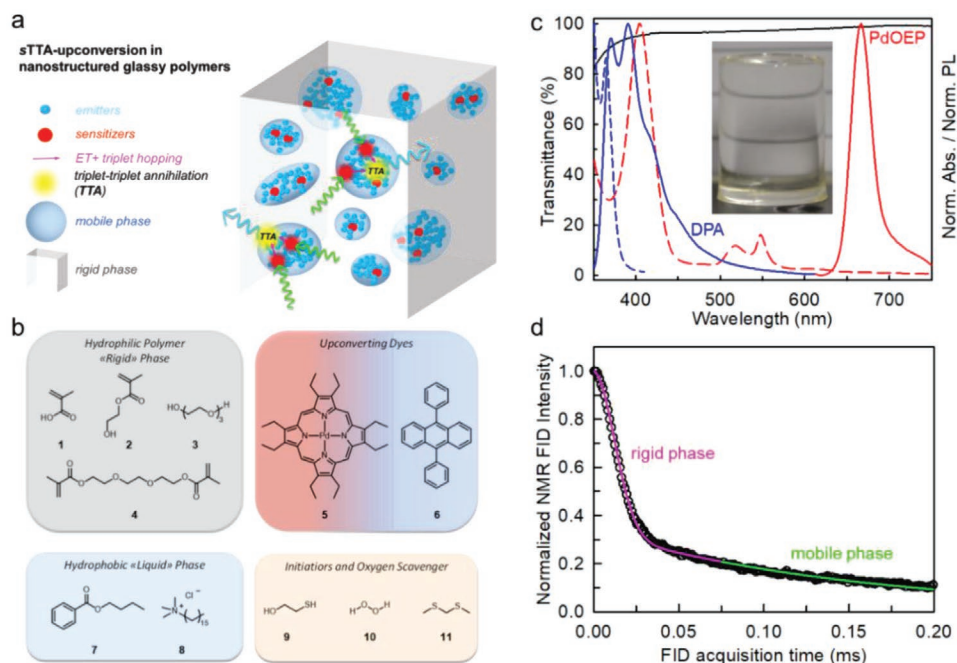


Figure 1. a) Schematic of the structure of the upconverting nanophase-separated polymer and of the confined sTTA-UC mechanism therein. b) Chemical structures of the green-to-blue upconverting polymer components. **1)** Methacrylic acid, **2)** 2-hydroxyethyl methacrylate, **3)** triethylene glycol, **4)** triethylene glycol dimethacrylate, **5)** Pd(II) octaethylporphyrin, **6)** 9,10-diphenylanthracene, **7)** butyl benzoate **8)** cetyltrimethylammonium chloride, **9)** 2-mercaptoethanol, **10)** H₂O₂, and **11)** dimethylthiomethane. c) Transmission spectrum of a dye-free nanophase-separated polymer sample (solid black line) superimposed to the absorption (dashed lines) and photoluminescence (PL, solid lines) spectra of the upconverting dyes employed, Pd(II) octaethylporphyrin (PdOEP, red) as sensitizer and 9,10-diphenylanthracene (DPA, blue) as annihilator/emitter. The inset is a digital picture of the dye-free nanophase-separated polymer. d) Time-domain NMR FID of the nanophase-separated polymer containing the upconverting dyes (DPA: PdOEP), acquired with MSE refocusing block at 303 K. The fit points out a fast Gaussian relaxation that characterizes the rigid phase and a slower exponential relaxation associated with the mobile phase.

protection from atmospheric oxygen. However, the materials displayed a somewhat limited stability in both the idle, as well as the operating state. Here, we introduce modifications to the concept that lead to significantly improved shelf- and operating lifetimes, while a high upconversion efficiency is maintained. We employed a bio-mimetic redox initiation system that permits the synthesis of such nanophase-separated polymers in a one-step process in air and the upconverting dyes primarily accumulate in the liquid domains whose average size is less than 50 nm (Figure 1a). The incorporation of the chromophores in these small liquid domains is achieved in high concentrations without detrimental phase segregation or aggregation effects. This enables both hopping-assisted ET and TTA and, importantly, an effective localization and confinement of interacting excitons, which has a direct impact on the sTTA-UC kinetics enhancing the upconversion performance at low power densities of the nanostructured polymer with respect to its homogeneous counterpart.^[6] The new upconverting nanomaterials show a remarkably high optical quality, an outstanding upconversion quantum yield QY_{uc} of ≈23%, and excellent stability in air, which is a prerequisite for the development of upconversion-based technologies.

2. Fabrication of Dyes-doped Nanostructured Glassy Polymers

The modifications reported here were motivated by the speculation that in the previously described nanostructured polymers

the decrease of the upconversion efficiency over time (in the idle state or under irradiation) were at least in part related to the degradation of the dyes due to reactions with trapped residues (such as oxygen, unreacted monomers, and initiators, as well as initiator decomposition products),^[7] instability of the morphology, and/or slow evaporation of the somewhat volatile solvent (1-tert-butyl-3,5-dimethyl benzene) that was used to form the liquid phase.^[5] Thus, we carried out a systematic investigation of how the various components influence the materials characteristics; as a result, we replaced the initiator system, surfactant, solvent and plasticizer, and incorporated an oxygen scavenger. Figure 1b shows the molecular structures of the moieties employed (1–11) to fabricate the upconverting nanophase-separated polymers (see Supporting Information). The novel redox initiation system used here was inspired by microbicidal mechanisms observed in immune cells, which produce HOCl and HOBr by an enzyme-catalyzed reaction of the corresponding halides with biosynthetic H₂O₂. The hypohalous acids then react with heteroatomic species present in the biological medium, notably thiols, and generate unstable halogenated intermediates that dissociate into radicals at room temperature.^[8] Speculating that this framework may permit one to carry out the polymerization under ambient conditions and that it would afford relatively inert residues, we chose to take advantage of the presence of halides (i.e., the counterion of the cetyltrimethylammonium surfactant) and a proton source (i.e., methacrylic acid) in our polymerization mixture to generate radicals in situ by sequentially adding H₂O₂ (10) and

a thiol to initiate the polymerization reaction (Figure S2, Supporting Information). 2-Mercaptoethanol (9, 2-ME) was chosen as a reducing agent, as it afforded transparent glasses with cetyltrimethylammonium bromide (CTAB) or chloride (CTAC) as a surfactant/halogen source. A mixture of the hydrophilic monomers methacrylic acid (1, MAA, 13% w/w), 2-hydroxyethyl methacrylate (2, HEMA, 53% w/w), and triethylene glycol dimethacrylate (4, TEG-diMA, 3.5% w/w) was employed to form the cross-linked, glassy polymer matrix upon free-radical polymerization. We proceeded by screening a series of ethylene glycol oligomers as plasticizers for the matrix, with the objective to minimize their evaporation (Table S1, Figure S3, Supporting Information) as well as a series of high boiling point hydrophobic solvents. Butyl benzoate (BuBz) was finally selected as hydrophobic solvent, since the use of compounds having even higher boiling points occasionally provoked macrophase segregation (Table S2, Supporting Information). Using the well-known TTA-UC sensitizer/emitter pair Pd(II) octaethylporphyrin (5, PdOEP) and 9,10-diphenylanthracene (6, DPA), a combination containing triethylene glycol (3, 15% w/w), BuBz (7, 10% w/w) and CTAC (8, 5% w/w) was empirically established as the system yielding the highest upconversion photoluminescence (UC-PL) intensity (Figure S4, Supporting Information). The nominal dye concentrations (Experimental Section) were 2×10^{-5} or 8×10^{-5} M for PdOEP and 1.5×10^{-2} M for DPA based on the total volume of the composition and assuming a density of 1 g mL^{-1} . However, due to preferred incorporation into the liquid phase (vide infra), the effective local concentration is much higher. The stability of freshly prepared samples was probed under continuous wave (cw) irradiation with incident light having a wavelength of 543 nm and a power density of 10 mW cm^{-2} . The UC-PL was observed to decrease continuously, which we speculated was due to residual oxygen reacting with the dyes. To verify this hypothesis, dimethylthiomethane (11, DMTM, 0.5% w/w) was incorporated in the mixture to act as a sacrificial oxygen scavenger,^[9] resulting in a dramatic improvement of the UC-PL stability (Figure S5 and Table S3, Supporting Information). All samples discussed below were therefore based on the composition containing the components reported thus far. The excellent optical quality of the polymerized mixture (Supporting Information) is demonstrated by the transmission spectrum and the picture of a dye-free sample shown in Figure 1c. In the visible spectral region between 400 and 700 nm, a dye-free nanophase-separated polymer sample with a thickness of 1 cm displayed an average transmittance of >90%, which in view of its structure is remarkable. The material features a glass transition temperature (T_g) of 50–52 °C (Figure S6, Supporting Information), which is in agreement with previous measurements of nanostructured poly(HEMA-co-MAA-co-TEG-diMA) plasticized with 15% w/w of ethylene glycol and lower than the T_g of the plasticizer-free copolymer of the same composition.^[5] The fact that the introduction of BuBz does not change the T_g is a first indication for the existence of well-separated domains of the rigid matrix polymer on the one hand and liquid solvent on the other (Figure S6, Supporting Information). Since we were not able to provide any evidence for microphase separation by electron microscopy, we carried out time-domain NMR experiments to confirm the presence of multiple phases. The proton magnetization

relaxation measurements reported in Figure 1d show bi-component relaxation dynamics that are indicative of the coexistence of mobile and rigid phases (Experimental Section).^[10] The analysis of spin diffusion experiments puts the average diameter of the mobile domains, which are assumed to be spherical, at $\approx 40 \text{ nm}$ (Figure S12, Supporting Information).^[11]

3. Upconversion Properties and Kinetics Analysis

The photophysical properties of the upconverting nanophase-separated polymers, the corresponding reference materials containing either DPA (1.5×10^{-2} M) or PdOEP (2×10^{-5} M), as well as a reference solution of DPA: PdOEP (10^{-2} M : 2×10^{-5} M) in BuBz were assessed by means of cw and time-resolved PL spectroscopy studies. Figure 2a shows the absorption spectra of the PdOEP and DPA: PdOEP doped nanophase-separated polymers prepared in quartz Suprasil cuvettes with an optical path length of 1 cm.

In the green spectral range of the visible spectrum, both samples feature the porphyrin characteristic absorption Q-band peaked at 540 nm. In the UV-blue region, the DPA molecules absorption saturates over 3 OD at wavelengths shorter than 400 nm (bottom panel), thus obstructing the second typical absorption band of porphyrins at 394 nm (top panel) and demonstrating the inclusion of both dyes in the host. Upon excitation at 532 nm, the PdOEP containing reference polymer shows the typical red phosphorescence (red-PL) with maximum at 670 nm. The corresponding time-resolved spectrum shows a single exponential decay with a characteristic lifetime $\tau_{ph} = 1.47 \text{ ms}$ (inset), suggesting that the sensitizer molecules experience a homogeneous environment due to negligible partitioning between the segregated phases.^[12] Identical features are observed in a PdOEP-containing polymer with the same concentration employed for making upconverters, thus excluding concentration-dependent competitive mechanisms (Figure S7c, Supporting Information). The DPA: PdOEP containing upconverting polymer exhibits a bright emission (blue-PL) upon excitation at 380 nm matching the DPA fluorescence,^[13] with a characteristic decay time $\tau_f = 10 \text{ ns}$ (inset). It behaves as a single exponential function demonstrating the absence of partitioning also for emitter molecules. It is worth noting that τ_f is independent of the system composition (Figure S7a, Supporting Information), thus demonstrating the absence of efficient parasitic deactivation channels due to the high amount of emitters employed or to the presence of the PdOEP sensitizers, such as a backwards Förster-type ET from upconverted DPA singlets to the porphyrin molecules. Upon excitation with laser light at 532 nm (Figure 2b), the PdOEP containing reference material shows an intense red PL (dashed line), while the DPA: PdOEP containing UC polymer displays bright blue UC-PL with a maximum at 435 nm (solid line). The occurrence of a TTA-based upconversion is demonstrated by the time-resolved PL data in Figure 2c (20 °C curve), which show that the UC-PL decay dynamics are orders of magnitude slower than DPA fluorescence, since the emitted light originates from the annihilation of long-living triplets.^[14] By comparing the integrated intensity of the red-PL with (I) and without (I_0) emitters, normalized by the sample absorbance at

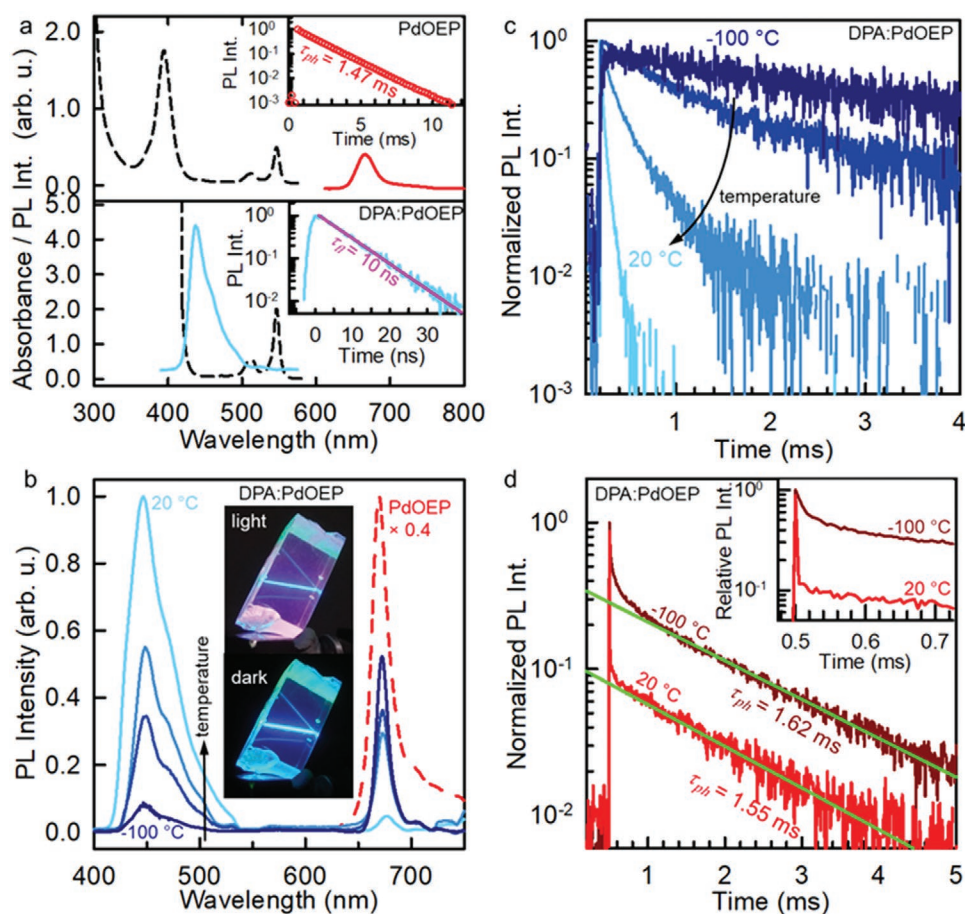


Figure 2. a) Absorption (dashed lines) and photoluminescence (PL) spectra (solid lines) of PdOEP doped (2×10^{-5} M, top) and DPA:PdOEP doped (1.5×10^{-2} M: 8×10^{-5} M, bottom) nanophase-separated polymers. The PL spectra were recorded under excitation at 532 nm and 380 nm, respectively. The top inset reports the time-resolved PL spectrum of the PdOEP containing reference polymer at 670 nm under pulsed excitation at 532 nm. The bottom inset shows the time-resolved PL spectrum of the DPA:PdOEP containing upconverting polymer at 435 nm under pulsed excitation at 405 nm. The time-resolved PL spectra were fitted with single exponential decay functions (solid lines). b) PL spectra of the DPA:PdOEP containing upconverting polymer under cw laser excitation at 532 nm (3 W cm^{-2}) as a function of temperature (20 °C, 5 °C, -20 °C, -100 °C). The dashed line shows the PL spectrum of the PdOEP containing reference polymer under the same excitation conditions at 20 °C. The inset shows digital pictures of a free-standing upconverting polymer sample under laser excitation at 532 nm taken under ambient light and in the dark. c) Time-resolved PL spectrum of the DPA:PdOEP containing polymer at 435 nm as a function of temperature (20 °C, 5 °C, -20 °C, -100 °C), under pulsed excitation at 532 nm at 10 Hz. d) Time-resolved PL spectrum of the DPA:PdOEP containing polymer at 670 nm under pulsed excitation at 532 nm at 20 °C and -100 °C. Solid lines are the fit of the long-time emission tails with a single exponential decay function. The inset is a magnification of the first millisecond of the explored temporal window.

532 nm (OD 0.25 and 0.08, respectively), we estimate an ET yield $\varphi_{ET} = (1 - I/I_0) \times 100 = 96\%$.^[12]

A correlation of the data acquired in cw experiments and the analysis of the time-resolved PL spectra provides information about the location of the dye molecules in the nanophase-separated host. As shown in Figure 2d, the time decay of the residual red-PL intensity is bi-exponential (20 °C curve). However, about 95% of the emission is quenched promptly ($<10 \mu\text{s}$), due to fast ET to DPA triplets, thus confirming the steady-state result that has revealed a high ET efficiency. Conversely, the negligible secondary slow component displays a characteristic lifetime of 1.55 ms, which suggests that a small fraction of the sensitizer molecules are incorporated in the rigid polymer phase, where ET in absence of closely situated emitter species is suppressed.^[15] It is worth noting that these results indicate that almost all PdOEP molecules are included and mixed with

the emitting species in the liquid domains, where collisional interactions such as Dexter ET and TTA can occur.^[16] Further insights into the dye arrangement within the liquid phase were obtained from temperature-dependent PL experiments. As shown in Figure 2b, at room temperature the cw PL spectrum of the DPA:PdOEP containing upconverting polymer recorded with excitation at 532 nm is dominated by UC-PL with negligible residual red-PL. Upon cooling the sample to -100 °C, that is, below the melting temperature of BuBz of -22 °C,^[17] the UC-PL intensity was reduced by one order of magnitude, while the red-PL intensity experienced a 7-fold increase that indicates a reduction of the ET yield to $\approx 10\%$. In the upconverting BuBz reference solution, the UC-PL almost disappeared when the sample was cooled to -100 °C and could only be detected at extremely high excitation intensities, while the sensitizer phosphorescence intensity grew almost two orders of magnitude

(Figure S8, Supporting Information) because the ET yield was reduced to zero upon crystallization of the solvent. The fact that the sTTA-UC process is not completely switched off in the nanophase-separated polymer is ascribed to the effective confinement of the dye molecules in small-volume domains so that at least some of them experience intermolecular distances as short as ≈ 2 nm, thus enabling both ET and TTA in the frozen sample at low powers without contribution of molecular translational diffusion.^[16] This description is in agreement with the estimated average intermolecular distance between DPA molecules of ≈ 2.6 nm calculated considering the increased dye concentration of $\approx 1.5 \times 10^{-1}$ M (see Supporting Information) reached after polymerization and confinement of chromophores in the liquid nanodomains (10% of the total volume according to the initial liquid-to-rigid feed ratio). Conversely, the strong phosphorescence enhancement and the UC-PL suppression seen in the frozen solution stem from the fact that the dyes are blocked at reciprocal distances much larger than typical Dexter ET radii, ≈ 6.0 nm at the given concentration of 10^{-2} M (see Supporting Information), with consequent inhibition of both ET and TTA.^[18]

This picture for the dyes arrangement within the nanostructured host is confirmed by time-resolved PL experiments. In the frozen BuBz reference solution, the red-PL decay time extends and reaches the value observed without emitters (Figure S7b, Supporting Information), thus demonstrating the absence of quantitative ET (Figure S8, Supporting Information). Yet, in the frozen polymer (Figure 2d), the quick drop of the red-PL intensity that marks the fast ET at 20 °C is only partially slowed down at -100 °C, indicating that hopping-mediated ET between excited PdOEPs and DPA molecules is possible. Moreover, in the UC polymer it is also possible to observe the typical slow sTTA-UC recombination dynamics (Figure 2c), that, at this temperature, occurs thanks to triplet exciton diffusion by hopping within the ensemble of close packed DPAs without the assistance of translational molecular motions. The progressive deceleration of both UC-PL intensity decay (Figure 2c) and rise time (Figure S9, Supporting Information) observed by lowering the temperature mirrors a decrease of the TTA rate k_{TTA} . Owing to a bimolecular process, this rate is set by the density of annihilating emitter triplets $[T]$ by $k_{TTA} = \gamma_{TT}[T]$, where γ_{TT} is the second order rate constant that characterizes the TTA process. The rate constant γ_{TT} is proportional to the triplet diffusivity,^[19] which according to literature^[20] in this case can be reduced also by the detrimental effect of the low temperature on the hopping-mediated diffusion within the disordered ensemble of dyes. Accordingly, the UC-PL intensity decay at -100 °C exhibits a single exponential behavior, meaning that the rate k_{TTA} , entirely governed by the hopping mechanism in this condition, is negligible with respect to the spontaneous triplet decay rate k_T (135 Hz at -100 °C, Figure S9, Supporting Information).^[14] Conversely, at room temperature the annihilation rate is large enough to dominate the recombination dynamics of the population of DPA triplets, thus maximizing the global conversion efficiency (vide infra.) It is worth noting that the UC-PL in the frozen system decays in the ms time range, as expected for unquenched DPA triplets (844 Hz at 20 °C in BuBz, Figure S10, Supporting Information).^[13] This demonstrates that nanodomains are a safe, defect-free environment for hopping triplets

and, importantly, that confined diffusing excitons are prevented to reach non-radiative recombination centers avoiding parasitic energy losses.

To highlight and understand the crucial consequences of a controlled dye-accumulation without segregation and aggregation on the sTTA-UC mechanism, we report in Figure 3a^[21] the different distributions of chromophores and their interaction in the upconverting reference solution—which is representative of other solutions as well as homogeneous solid materials—and in the nanophase-separated polymers, as indicated by the PL experiments. Firstly, a localized, efficient sensitization of triplets can be achieved in the dye-containing nanodomains of the nanostructured polymer, where both ET and TTA occur by hopping-assisted diffusion of triplet excitons. Secondly, most importantly, the confinement of sensitizers implies that in the nanostructured polymer the average mean distance at which two triplets are generated is much shorter than in materials that contain the same concentration of dye molecules in a homogeneously placed manner; as a result, the TTA rate is intrinsically enhanced and the conversion efficiency approaches its maximum at a lower excitation intensity. In order to provide further evidence for this analysis, the upconversion performance of a nanostructured polymer was measured and compared with that of a BuBz solution containing the same amount of dyes. Figure 3b shows the upconversion quantum yield QY_{uc} measured as a function of the incident excitation intensity I_{exc} at 532 nm. The energy-conservation limit sets the maximum QY_{uc} achievable as large as 0.5 (see Supporting Information, Section 1). In both cases, the QY_{uc} increases with I_{exc} and levels off at a maximum of $23 \pm 3\%$, which matches the maximally achievable value considering the limit imposed by the spin statistical probability of singlet generation upon TTA.^[16]

Remarkably, the stability check data reported in Figure 3c show that the nanophase-separated polymer does not suffer from significant efficiency losses ($<10\%$) after storing the sample for more than 3 months, a striking result if compared to the previously observed loss of $\approx 50\%$ in half of this time span.^[5] Conversely, the reference solution loses its upconversion ability completely within ten days, thus demonstrating the excellent oxygen shielding effect of the polymer host. Similar results were obtained for nanophase-separated upconverting polymers containing two other upconverting dye pairs (for red-to blue and NIR-to-visible upconversion, Supporting Information), validating the versatility of the designed synthetic strategy to fabricate in air industrially processable upconverters. The oxygen transmission rate (OTR) of the upconverting nanostructured polymer (Table S4, Supporting Information) was indeed found to be comparable to poly(ethylene terephthalate) and polyamide 6, that is, technologically used polymers that are known to provide a substantial protection from atmospheric oxygen.^[22,23] A careful analysis of the QY_{uc} versus I_{exc} data shows an additional interesting peculiarity of the sTTA-UC process in the nanophase-separated polymer in respect to the reference solution. Usually, the sTTA-UC efficiency plateaus to a constant value at high excitation powers, because in this regime the TTA process becomes the most efficient recombination channel for emitter triplets ($k_{TTA} \gg k_T$), thus the TTA yield is equal to unity and QY_{uc} is maximal. Conversely, at low powers the TTA is negligible ($k_{TTA} \ll k_T$) and QY_{uc} depends linearly on I_{exc} , as expected

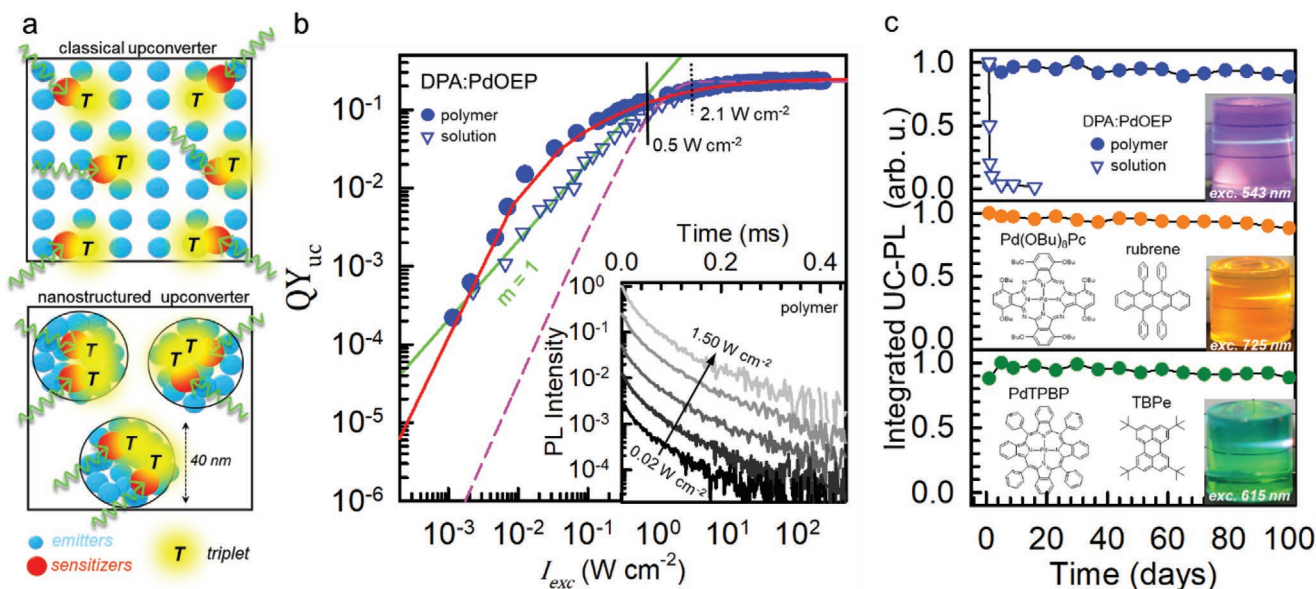


Figure 3. a) Schematic of the distribution of upconverting chromophores and triplet excitons, upon absorption of green photons, in a “classical” upconverting material in which the dye molecules are homogeneously distributed, and a nanophase-separated polymer with the same volume and number of chromophores. b) sTTA-upconversion quantum yield (QY_{uc}) of the DPA:PdOEP ($1.5 \times 10^{-2} \text{ M} : 8 \times 10^{-5} \text{ M}$) containing nanophase-separated polymer (circles) and the reference DPA:PdOEP ($1.5 \times 10^{-2} \text{ M} : 8 \times 10^{-5} \text{ M}$) solution in BuBz (triangles) as a function of the incident excitation intensity I_{exc} at 532 nm. Short vertical lines mark the excitation intensity threshold I_{th} , that is, where QY_{uc} is half of its maximum value (solid line for the polymer, dashed line for the solution). In the case of the solution, the solid line is the fit of the low-power data with a straight line with slope $m = 1$. In the case of the nanophase-separated polymer, the fit of data was obtained by calculating QY_{uc} for an ensemble of nanoemitters activated at different excitation intensities according to a size-dependent binomial statistics of excitation energy distribution (red solid line). The size distribution was assumed to be log-normal with a fitted mean diameter of 48 nm. The dashed line is the efficiency dependency on I_{exc} calculated assuming a binomial distribution of the excitation energy on a homogenous population of spherical UC nanodomains with a diameter of 40 nm. Inset: time-resolved PL spectra of the DPA:PdOEP containing nanophase-separated polymer at 435 nm under a modulated 532 nm laser excitation at different powers. c) Integrated intensity of the UC-PL measured under excitation with a Xe lamp over a prolonged period for nanostructured polymers containing DPA:PdOEP (top, $1.5 \times 10^{-2} \text{ M} : 8 \times 10^{-5} \text{ M}$, $\lambda_{exc} = 543 \text{ nm}$), rubrene: Pd(OBu)₈Pc (mid, $\lambda_{exc} = 725 \text{ nm}$), and TBPc: PdTPBP (bottom, $\lambda_{exc} = 615 \text{ nm}$) as upconverting dye pairs, respectively. All measurements were performed on samples prepared under ambient conditions and kept in glass cuvettes sealed with a polymer film. The insets show pictures of the respective materials exhibiting upconversion. For comparison, the top panel reports the same measurement for the DPA:PdOEP solution in BuBz (triangles).

for bimolecular processes. The excitation intensity that marks the half of the maximum QY_{uc} is defined here as the excitation threshold I_{th} .^[24] This phenomenology is clearly observed in the present reference solution, where I_{th} is 2.0 W cm^{-2} . However, in the case of the QY_{uc} of the nanophase-separated polymer, the saturation to the maximum is clearly super-linear, thus allowing to reach the threshold at 0.5 W cm^{-2} , that is, at a four times lower excitation intensity than that of the reference solution.

The peculiar dependence of the upconversion efficiency on I_{exc} is a fingerprint of a TTA process occurring in confined systems when triplets are physically confined in discrete volumes that are smaller than the space potentially explored by their random diffusion. When two emitter triplets are simultaneously created in such a confined space, they can decay only by annihilation with a resulting TTA efficiency of 100%^[25] and potentially reach the maximum conversion efficiency at excitation intensities lower than in the classical bulk counterpart.^[6] The occurrence of confined-TTA in the nanostructured host is demonstrated by the time-resolved PL data shown in the inset of Figure 3b. In contrast to the bulk-TTA regime, where the excitation intensity determines k_{TTA} and the UC-PL signal decay dynamics,^[14] no changes in the UC-PL time-resolved spectrum are observed when I_{exc} is varied by two orders of magnitude

around I_{th} . Specifically, the UC-PL intensity dynamics, which mirrors the triplet lifetime, shows an average lifetime $\tau_{UC} = 2 \times 10^{-2} \text{ ms}$, calculated as the time when the time-zero intensity decreases by a factor $1/e$. The corresponding average decay rate is $k_{UC} = (\tau_{UC})^{-1} \approx 50 \text{ kHz}$. This value is significantly larger than the triplet spontaneous decay rate $k_T = 844 \text{ Hz}$, which implies $k_{UC} \approx k_{TTA}$ and, provided that at least two triplets are generated in the same confined volume, a power-independent TTA efficiency $\phi_{TTA}[\%] = \frac{k_{TTA}}{k_{TTA} + k_T} \times 100 \approx 100\%$. This finding

is consistent with the confined-TTA process. An increase of I_{exc} leads to a growth of the number of isolated nanodomains that contain at least one triplet pair. Triplet pairs in independent nanodomains annihilate efficiently with the same probability without affecting the global recombination dynamics of the upconverted emission. More importantly, the achieved confinement of the annihilating triplet excitons shortens their average intermolecular distance, enhancing their annihilation probability and therefore the upconversion efficiency at low powers, thus reducing the excitation threshold with respect to the solution case.

As suggested by the spin-diffusion experiments, the cw and time-resolved PL data analysis infers therefore the presence of non-interacting upconverting nanostructures where

confined-TTA occurs because their sizes are significantly smaller than the DPA triplet diffusion length of 463 nm (see Supporting Information). This is the first observation of such a phenomenon in bulk materials, and, interestingly, the results obtained infer some differences with respect to the case of upconverting nanoparticles. Specifically, it is worth noting that the QY_{uc} versus I_{exc} behavior in our new nanophase-separated polymers differs from the one of previously reported nano-upconverters, which strictly follows a binomial distribution of the excited states (Figure 3b, dashed line).^[6] This discrepancy can be ascribed to the fact that the polymer nanostructuring is a homogenous process, which results in a log-normal distribution of the liquid domain size.^[26] In order to analyze the QY_{uc} dependence on I_{exc} , and to extrapolate the size distribution of the liquid domains in the polymer matrix, we analyzed the power-dependent efficiency data with a statistical approach. Assuming a confined-TTA process, the overall emission intensity was obtained by adding the number of upconverted photons generated in every UC-active nanodomain, that is, simultaneously containing at least two triplets, whose number progressively increases as the excitation intensity raises the number of excitons available in the system. The UC-activation threshold of each domain is set by the probability to contain simultaneously two triplets and it is determined by its size.^[6] Therefore we modeled the nanophase-separated polymer as an ensemble of nano-upconverters that are activated at different powers according to a size-determined binomial statistics of the excitation energy distribution (Figure 3b, Supporting Information). As reported in Figure 3b, the observed power-dependent behavior of the upconversion efficiency is perfectly reproduced (solid line) by considering the confined-TTA upconversion dynamics occurring in a log-normal distribution of spherical domains with a mean diameter of ≈ 48 nm (Figure S11, Supporting Information). This result is in excellent agreement with the data obtained from time-resolved NMR measurements, thus further confirming the intrinsic nanostructured architecture of the material and highlighting the crucial role of nanostructuring in setting the material macroscopic upconversion properties.

4. Conclusions

In conclusion, we successfully fabricated sTTA-based upconverting nanostructured rigid polymers that exhibit an excellent upconversion yield of more than 20%, which is comparable to that of the best solution-based systems and close to the theoretical limit. The employed synthetic route allows creating such materials in a simple one-pot procedure in air and the materials show excellent stability. In these materials, efficient electronic interactions between upconverting moieties is achieved by embedding the chromophores in isolated, nanosized liquid domains within the rigid host polymer. The co-localization of sensitizers and emitters increases their local density to extremely high values without partitioning or aggregation effects that could affect the optical quality of the material, thus enabling ET and TTA by molecular diffusion supported by hopping-mediated energy migration. Moreover, the confinement of triplet exciton pairs in non-communicating domains

enables the upconversion process to work in a protected defect-free environment, thus avoiding trivial energy losses, and to reach the confined-TTA regime where the annihilation yield is maximized independently of the excitation intensity. It is worth noting that the effective local increase of the triplet exciton density leads to an enhanced upconversion performance of the new nanomaterials at lower incident powers with respect to the corresponding liquid solution. These results strongly support nanostructuring as a general strategy to overcome the limitations on the synthesis of highly doped bulk upconverters. The model developed suggests indeed that controlled nanostructuring is a powerful design concept to manipulate safely the local density of dyes in solid systems and, at the same time, to tune the sTTA-UC dynamics in order to reach the ultralow upconversion thresholds. The best trade-off between nanostructure size and energy distribution probability, together with an enhanced absorption by including larger amount of sensitizers, will enable indeed to achieve high-efficiency upconverting polymers at excitation intensities well below the solar irradiance. Considering their striking stability and mechanical properties, the compatibility of the fabrication route with straightforward and readily scalable processes, and the possibility to incorporate a priori any dye pair according to the application demands, these materials appear to be appealing for technological applications.

5. Experimental Section

Preparation of Dye-Free Nanophase-Separated Polymers: Chemicals were purchased from Sigma-Aldrich, ABCR, Acros Organics, TCI (Tokyo Chemical Industry Co., Ltd.) or Inochem, Ltd. (Frontier Scientific, Inc) and were used as received. A 20 mL vial equipped with a stir bar was charged under ambient conditions with cetyltrimethylammonium chloride (250 mg), 2-hydroxyethyl methacrylate (2.66 g), methacrylic acid (665 mg), triethylene glycol dimethacrylate (175 mg), butyl benzoate (500 mg), and triethylene glycol (750 mg). The mixture was heated in an oil bath to 80 °C and stirred for 20 min to appear clear and homogeneous. The mixture was then removed from the oil bath and an aqueous solution of H₂O₂ (30%, 10 mg) and 2-mercaptoethanol (10 mg) were subsequently added. The mixture was briefly shaken and allowed to react for 1–2 min before dimethylthiomethane (27 mg) was added and the mixture was shaken again. The final mixture was filtered warm through a 0.2 μ m PTFE-filter into either an optical glass cuvette or a 10 mL glass vial. The still clear mixture was left overnight at room temperature to obtain a transparent, hard material, which was either kept in a polymer film sealed cuvette and used for quantitative optical measurements or released from the glass vial by breaking the latter with a hammer.

Material Characterization: Differential scanning calorimetry measurements were performed using a Mettler-Toledo DSC-1 equipped with a Huber TC100 cooling regulation system. Scanning electron microscopy. The ultrastructure was investigated with a MIRA 3 LMH field-emission electron microscope (Tescan, Brno, Czech Republic). To prevent charging, the samples were sputter-coated by a 2 nm thin layer of Pt/Pd (80:20) alloy prior to imaging. OTR measurements were performed on triplicates of ≈ 0.2 mm thick nanophase-separated polymer films with a Mocon OX-TRAN MH 2/20 and SH 2/20 according to the standard ASTM F1927-14. Time domain ¹H-NMR measurements were performed on a 0.5 T Bruker Minispec mq20 instrument with proton Larmor frequency of 19.9 MHz, equipped with a static probe and a BVT3000 heater temperature control unit working with nitrogen gas. The temperature was calibrated using an external thermometer with an accuracy of 1 K. The precision is 0.1 K and the temperature is stable within that range during the measurement. The samples were

left around ten minutes in the magnet to ensure thermal equilibration before starting the experiments. FIDs for rigid phase determination were acquired after a pulsed mixed magic sandwich echo (MSE) was performed on each sample with 128 scans. Domain size calculations were performed on FIDs collected after a MSE refocused Goldman-Shen sequence, using the initial rate approximation for the sink (rigid) region. The receiver dead time was set to 12.7 μs , and phase switching time to 2.2 μs while the 90° pulse length was set to 2.10 μs .

Optical Studies: UV–vis absorption spectra were recorded on a Shimadzu UV-2401PC or on a Cary Varian 50 spectrometer. The concentration of the dyes in the materials was determined by optical absorption measurements and using the Lambert-Beer law and the molar extinction coefficients of the sensitizer and the emitter (Figure S13, Supporting Information). Steady-state PL spectra were acquired with a Photon Technology International C720 spectrophotometer equipped with a Hamamatsu R928P photomultiplier or with a nitrogen cooled charge-coupled device (Spex \approx 2000) coupled to a polychromator Triax 190 from J-Horiba. Green-to-blue upconversion spectra were recorded using a 2 mW non-polarized 543 nm helium–neon (HeNe, 543 nm) laser (Thorlabs HGR020) or a focused doubled Nd:YAG diode pumped Coherent Verdi TEM 00 CW laser at 532 nm for excitation. 1/e² beam diameters of 0.83 mm (HeNe) or 0.80 mm (Nd:YAG) were measured by the knife blade method. The laser intensity was varied using reflective power density neutral filters and measured with an optical power meter (Thorlabs PM100USB, power sensor S120VC). The excitation light was removed by using line filters, while for detection the laser stray light was attenuated with a notch filter. For the red-to-blue, red-to-green, and dark-red-to-yellow upconversion, a 635 or a 670 nm solid-state laser diode from Roithner Lasertechnik was used as excitation source. All spectra were corrected for the instrumental optical response. For time-resolved upconversion measurements, the samples were excited at 532 nm by modulating a Nd:YAG laser with a TTI TG5011 wavefunction generator. The spectra were recorded by nitrogen cooled photomultiplier (Hamamatsu R5509-73) coupled with a high-speed amplifier (Hamamatsu C5594), a 74 100 Cornerstone 2601/4 (ORIEL) monochromator, and a PCI plug-in multichannel scaler ORTEC 9353 100 ps time digitizer/MCS in a photon counting acquisition mode. Fluorescence and phosphorescence time-resolved spectra as a function of temperature were obtained by using the II harmonic of Nd:YAG Continuum Minilite laser (10 ns pulse width), detecting the luminescence decay by an Edinburgh LP90 flash photolysis setup. The sTTA-UC quantum yield (QY_{UC}) of the DPA:PtOEP upconverting nanophase-separated polymer was measured with respect to a standard reference solution of PtOEP (Pt(II) octaethylporphyrin, 10^{−4} M) and DPA (10^{−2} M) in THF, whose QY_{UC} is known (see Supporting Information for details).

Supporting Information

Supporting Information is available from the Wiley Online Library or from the author.

Acknowledgements

F.S. and A.R. contributed equally to this work. Financial support from BASF, BASF Schweiz, the Italian Ministry of University and Research (MIUR) through grant Dipartimenti di Eccellenza–2017 “Materials for Energy”, and the Adolphe Merkle Foundation is gratefully acknowledged. R.V. acknowledges funding received from the European Union under the H2020 Marie Skłodowska-Curie Actions grant agreement No 752143. The authors thank Drs. Maik Schlesinger and Andreas Hafner for valuable discussions.

Conflict of Interest

The employer of F.S. and C.W. has been granted patents that protect nanophase-separated upconverting polymers.

Keywords

nanostructured polymers, photon upconversion, sensitized triplet–triplet annihilation, wavelength shifting

Received: May 25, 2020

Revised: August 30, 2020

Published online:

- [1] a) T. Trupke, A. Shalav, B. S. Richards, P. Würfel, M. A. Green, *Sol. Energy Mater. Sol. Cells* **2006**, *90*, 3327; b) T. N. Singh-Rachford, F. N. Castellano, *Coord. Chem. Rev.* **2010**, *254*, 2560; c) G. J. Christoph, F. Stefan, *Adv. Opt. Mater.* **2015**, *3*, 510; d) J. C. Goldschmidt, S. Fischer, *Adv. Opt. Mater.* **2015**, *3*, 510.
- [2] S. Balushev, T. Miteva, V. Yakutkin, G. Nelles, A. Yasuda, G. Wegner, *Phys. Rev. Lett.* **2006**, *97*, 143903.
- [3] Y. C. Simon, C. Weder, *J. Mater. Chem.* **2012**, *22*, 20817.
- [4] a) P. Duan, D. Asthana, T. Nakashima, T. Kawai, N. Yanai, N. Kimizuka, *Faraday Discuss.* **2017**, *196*, 305; b) J.-H. Kim, F. Deng, F. N. Castellano, J.-H. Kim, *Chem. Mater.* **2012**, *24*, 2250; c) R. Vadrucci, C. Weder, Y. C. Simon, *J. Mater. Chem. C* **2014**, *2*, 2837; d) R. Vadrucci, C. Weder, Y. C. Simon, *Mater. Horiz.* **2015**, *2*, 120; e) C. Li, C. Koenigsmann, F. Deng, A. Hagstrom, C. A. Schmuttenmaer, J.-H. Kim, *ACS Photonics* **2016**, *3*, 784; f) A. Monguzzi, A. Oertel, D. Braga, A. Riedinger, D. K. Kim, P. N. Knüsel, A. Bianchi, M. Mauri, R. Simonutti, D. J. Norris, F. Meinardi, *ACS Appl. Mater. Interfaces* **2017**, *9*, 40180; g) K. Kamada, Y. Sakagami, T. Mizokuro, Y. Fujiwara, K. Kobayashi, K. Narushima, S. Hirata, M. Vacha, *Mater. Horiz.* **2017**, *4*, 83; h) J. Park, M. Xu, F. Li, H.-C. Zhou, *J. Am. Chem. Soc.* **2018**, *140*, 5493; i) J. Perego, J. Pedrini, C. X. Bezuidenhout, P. E. Sozzani, F. Meinardi, S. Bracco, A. Comotti, A. Monguzzi, *Adv. Mater.* **2019**, *31*, 1903309; j) T. Ogawa, N. Yanai, A. Monguzzi, N. Kimizuka, *Sci. Rep.* **2015**, *5*, 10882; k) P. Duan, N. Yanai, H. Nagatomi, N. Kimizuka, *J. Am. Chem. Soc.* **2015**, *137*, 1887; l) S. H. C. Askes, V. C. Leeuwenburgh, W. Pomp, H. Arjmandi-Tash, S. Tanase, T. Schmidt, S. Bonnet, *ACS Biomater. Sci. Eng.* **2017**, *3*, 322; m) C. Wohnhaas, K. Friedemann, D. Busko, K. Landfester, S. Balushev, D. Crespy, A. Turshatov, *ACS Macro Lett.* **2013**, *2*, 446; n) O. S. Kwon, J.-H. Kim, J. K. Cho, J.-H. Kim, *ACS Appl. Mater. Interfaces* **2015**, *7*, 318; o) S. N. Sanders, M. K. Gangishetty, M. Y. Sfeir, D. N. Congreve, *J. Am. Chem. Soc.* **2019**, *141*, 9180.
- [5] R. Vadrucci, A. Monguzzi, F. Saenz, B. D. Wilts, Y. C. Simon, C. Weder, *Adv. Mater.* **2017**, *29*, 1702992.
- [6] F. Meinardi, M. Ballabio, N. Yanai, N. Kimizuka, A. Bianchi, M. Mauri, R. Simonutti, A. Ronchi, M. Campione, A. Monguzzi, *Nano Lett.* **2019**, *19*, 2169.
- [7] a) J. Lal, R. Green, *Journal of Polymer Science* **1955**, *17*, 403; b) R. Bowen, H. Argentar, *The Journal of the American Dental Association* **1967**, *75*, 918.
- [8] a) M. J. Davies, C. L. Hawkins, *Free Radical Res.* **2000**, *33*, 719; b) C. L. Hawkins, B. E. Brown, M. J. Davies, *Arch. Biochem. Biophys.* **2001**, *395*, 137.
- [9] D. Dzebo, K. Moth-Poulsen, B. Albinsson, *Photochem. Photobiol. Sci.* **2017**, *16*, 1327.
- [10] a) A. Maus, C. Hertlein, K. Saalwächter, *Macromol. Chem. Phys.* **2006**, *207*, 1150; b) M. Mauri, L. Mauri, V. Causin, R. Simonutti, *Anal. Methods* **2011**, *3*, 1802; c) S. Bonetti, M. Farina, M. Mauri, K. Koynov, H. J. Butt, M. Kappl, R. Simonutti, *Macromol. Rapid Commun.* **2016**, *37*, 584.
- [11] M. Mauri, Y. Thomann, H. Schneider, K. Saalwächter, *Solid State Nucl. Magn. Reson.* **2008**, *34*, 125.
- [12] J. R. Lakowicz, *Principles of Fluorescence Spectroscopy*, 3rd ed. Springer, New York **2006**.

- [13] M. Montalti, A. Credi, L. Prodi, M. T. Gandolfi, J. Michl, V. Balzani, *Handbook of photochemistry*, CRC Press, Boca Raton, Fla., London, New York, N.Y. **2006**.
- [14] Y. Y. Cheng, B. Fückel, T. Khoury, R. G. C. R. Clady, M. J. Y. Tayebjee, N. J. Ekins-Daukes, M. J. Crossley, T. W. Schmidt, *J. Phys. Chem. Lett.* **2010**, *1*, 1795.
- [15] "Porphyrin Handbook: Multiporphyrins, Multiphthalocyanines and Arrays", **2003**.
- [16] A. Monguzzi, R. Tubino, F. Meinardi, *Phys. Rev. B* **2008**, *77*, 155122.
- [17] M. J. O'Neil, P. E. Heckelman, P. H. Dobbelaar, K. J. Roman, C. M. Kenny, L. S. Karaffa, C. *Royal Society of, The Merck index : an encyclopedia of chemicals, drugs, and biologicals*, Royal Society of Chemistry, Cambridge, UK **2013**.
- [18] a) D. L. Dexter, *J. Chem. Phys.* **1953**, *21*, 836; b) M. Inokuti, F. Hirayama, *J. Chem. Phys.* **1965**, *43*, 1978; c) A. Köhler, H. Bässler, *J. Mater. Chem.* **2011**, *21*, 4003.
- [19] J. Jortner, S.-I. Choi, J. L. Katz, S. A. Rice, *Phys. Rev. Lett.* **1963**, *11*, 323.
- [20] L. Grisanti, Y. Olivier, L. Wang, S. Athanasopoulos, J. Cornil, D. Beljonne, *Phys. Rev. B* **2013**, *88*, 035450.
- [21] J. Zimmermann, R. Mulet, G. D. Scholes, T. Wellens, A. Buchleitner, *J. Chem. Phys.* **2014**, *141*, 184104.
- [22] V. Siracusa, L. Genovese, C. Ingrao, A. Munari, N. Lotti, *Polymers* **2018**, *10*.
- [23] J. Lange, Y. Wyser, *Packaging Technology Science* **2003**, *16*, 149.
- [24] A. Monguzzi, J. Mezyk, F. Scotognella, R. Tubino, F. Meinardi, *Phys. Rev. B* **2008**, *78*, 195112.
- [25] A. Monguzzi, M. Mauri, M. Frigoli, J. Pedrini, R. Simonutti, C. Larpent, G. Vaccaro, M. Sassi, F. Meinardi, *J. Phys. Chem. Lett.* **2016**, *7*, 2779.
- [26] a) J. Söderlund, L. B. Kiss, G. A. Niklasson, C. G. Granqvist, *Phys. Rev. Lett.* **1998**, *80*, 2386; b) E. Limpert, W. Stahel, M. Abbt, *BioScience* **2001**, *51*, 341.